

# Dynamic Contact Angle Reformulates Pore-Scale Fluid-Fluid Displacement at Ultralow Interfacial Tension

Weipeng Yang and Chenliang Fu, University of Tulsa; Yujing Du, University of Texas at Austin; Ke Xu, Peking University; Matthew T. Balhoff, University of Texas at Austin; and Javen Weston and Jun Lu\*, University of Tulsa

## Summary

Surfactant flooding is an effective enhanced oil recovery method in which the oil/water interfacial tension (IFT) is reduced to ultralow values ( $<0.01$  mN/m). The microscopic fluid-fluid displacement has been extensively studied at high IFT ( $>10$  mN/m). However, the microscopic displacement dynamics can be significantly different when the IFT is ultralow because the dynamic contact angle increases with the increase of the capillary number. In this study, surfactant flooding was performed and visualized in micromodels to investigate the dynamics of multiphase displacement at ultralow IFT. Although the micromodels used were strongly water-wet, the displacements of oil by surfactant solutions at ultralow IFT appeared as drainage. Furthermore, a macroscopic oil film was left behind on the surface, which indicates that a contact line instability occurred during displacements. The shape of the oil/water meniscus was determined by the balance between viscous forces and capillary forces. The meniscus can be significantly distorted by viscous forces at ultralow IFT. Therefore, the water-wet micromodel exhibits an oil-wet behavior at ultralow IFT, and the displacements of oil by surfactant solutions at ultralow IFT manifested as drainage rather than imbibition. The flow behavior is further complicated by the spontaneous formation of microemulsion during displacement. The microemulsion is mainly formed from the residual oil. The formation of a microemulsion bank made the surfactant solution discontinuous, with transport in the form of droplets in the microemulsion bank and displacement front. The novelty of this work is to reveal the effects of dynamic contact angle on the ultralow IFT displacement.

## Introduction

Surfactant flooding has been used in many subsurface applications including enhanced oil recovery, nonaqueous phase liquid remediation, and more (Zhong et al. 2003; Johannessen and Spildo 2013; Lu et al. 2014a; Lu and Pope 2017). The added surfactant in injection water reduces the oil/water IFT and alters the rock wettability, which leads to increased oil recovery (Hirasaki et al. 2011; Kathel and Mohanty 2013). Oil ganglia are trapped by capillary pressure in pores after primary or secondary recovery. By reducing the IFT between oil and water, the capillary pressure is significantly reduced, and then the trapped oil can be mobilized. The dimensionless capillary number ( $Ca = v\mu/\gamma$ , where  $v$  and  $\mu$  are the velocity and viscosity of injected fluid, respectively, and  $\gamma$  is the IFT between two phases) is the ratio of viscous to capillary forces. The  $Ca$  is correlated with the oil recovery, and the preceding certain values of  $Ca$  lead to almost a complete oil recovery. Chatzis and Morrow (1984) showed that the values of the capillary number to achieve complete oil recovery are approximately  $1.5 \times 10^{-3}$ . However, the capillary number during conventional waterflooding is on the order of magnitude of  $10^{-6}$ , which is well below this value (Foster 1973). Increasing the water injection rate by  $10^3$  times is not feasible, but the IFT between oil and water can be reduced to ultralow values ( $<0.01$  mN/m) by using a well-formulated surfactant system. Although there is a great potential to enhance oil or nonaqueous phase liquid recovery by applying surfactant flooding, the multiphase displacement at ultralow IFT on the scale of individual pores has been less studied than that at high IFT. It is questionable whether the governing factors of high IFT displacement, especially wettability, are still important in ultralow IFT displacement. A better understanding of the microscopic displacement dynamics is essential to design a successful pilot test and accurately model the fluid flow in the reservoir.

Capillary-dominated, two-phase immiscible displacement at high IFT in 2D porous media has been extensively studied (Lenormand et al. 1983; Cieplak and Robbins 1988, 1990; Jung et al. 2016). The immiscible displacement in porous media is governed by many factors, such as viscosity, capillary number, wettability, pore geometry, and heterogeneity of the porous media (Holtzman and Segre 2015; Singh et al. 2019). The typical advance modes of the oil/water meniscus in porous media are burst, touch, and overlap, corresponding to different types of interfacial instability (Cieplak and Robbins 1988). The structure and evolution of the displacement front is controlled by the interfacial instability, which is strongly related to the wettability of porous media (Jung et al. 2016). The oil/water displacements in porous media are generally described as imbibition and drainage depending on the wettability. The capillary forces are driven forces of imbibition because of the concave oil/water meniscus, and the water can be spontaneously drawn into porous media (Morrow and Mason 2001). Whereas in drainage, the capillary forces hinder the entrance of water into porous media because of the convex oil/water meniscus (Lenormand et al. 1983). By changing the wettability of a micromodel over a wide range of contact angles, Zhao et al. (2016) showed that the displacement pattern can transition from ramified to compact by increasing the micromodel's affinity to the invading fluid until a threshold contact angle. Because wettability is one of the key factors that affects the displacement pattern and efficiency, efforts have been made to modify the wettability of porous media to change displacements from drainage to imbibition to maximize oil recovery (Gupta and Mohanty 2008; Mahani et al. 2015; Bartels et al. 2017; Abedi et al. 2020).

Typically, the wettability of a material is determined by measuring the contact angle under static conditions, and this value is also used for modeling fluid flow in porous media. When the capillary number is low, the apparent contact angle during two-phase displacement is close to the static contact angle. However, the oil/water meniscus can be distorted by viscous forces at high capillary number, which can make the dynamic contact angle significantly larger than the static contact angle (Hoffman 1975; Fermigier and Jenffer 1991; Blake et al. 1999). For ultralow IFT displacement, the capillary number is significantly increased because of the dramatic reduction of IFT. In this scenario, the capillary force is relatively weak and dominated by viscous forces, making the dynamic contact angle

\*Corresponding author; email: jun-lu@utulsa.edu

Copyright © 2021 Society of Petroleum Engineers

Original SPE manuscript received for review 4 August 2020. Revised manuscript received for review 25 September 2020. Paper (SPE 204459) peer approved 7 October 2020.

significantly larger than the static contact angle (Hansen and Toong 1971; Ngan and Dussan V. 1982). The initial concave meniscus becomes convex at high capillary number (Fermigier and Jenffer 1991; Blake et al. 1999), which is expected to significantly change the displacement pattern and phase distribution in the capillary tube and porous media compared to those of low capillary number. When the capillary number is large enough, the dynamic contact angle for the invading phase can reach  $180^\circ$ , making the three-phase contact line unstable, which leads to the entrainment of the defending phase (Marchand et al. 2012). Thus, fluid-fluid displacements at high capillary number appear as strong drainage, regardless of static contact angle, which leads to the undesired ramified displacement patterns at unfavorable viscosity ratios. To the best of our knowledge, the concept of dynamic contact angle has not been considered in existing studies of ultralow IFT surfactant flooding.

It is generally believed that reducing the oil/water IFT is helpful to enhance oil recovery. However, if the contact line becomes unstable with the decrease of IFT, the defending phase will remain on the pore surface, resulting in the pore-scale displacement efficiency lower than that when contact line is stable (corner flow is not considered here) (Marchand et al. 2012). Meanwhile, the wettability alteration is widely accepted to be an important mechanism of surfactant flooding. Therefore, if the dynamic contact angle is significantly larger than the static contact angle because of the ultralow IFT, the surfactant flooding will manifest as strong drainage even in an initial strongly water-wet reservoir. Consequently, it is questionable whether it is meaningful to discuss the effects of wettability alteration in ultralow IFT displacement, at least at the displacement front. Therefore, some key questions need to be answered to better understand the ultralow IFT displacement: How does the dynamic contact angle change compared to the static contact angle in ultralow IFT surfactant flooding? How will the dynamic contact angle affect the distribution of each phase in the pores during the displacement? What are the roles of the dynamic and static contact angles in the displacement, respectively? With the help of the microfluidic technique, surfactant flooding with ultralow IFT has been visualized and studied by many researchers. Mejia et al. (2019) conducted surfactant flooding in oil-wet micromodel with fractures. They observed that the wettability alteration is a relatively slow process, and wettability varies between pores. Howe et al. (2015) carried out surfactant flooding with two different IFTs in a homogeneous oil-wet micromodel. An intriguing phenomenon that can be found is that the oil/surfactant interface is more convex when oil is displaced by surfactant solution with lower IFT. Moreover, the wettability alteration can be observed when oil was displaced at higher IFT rather than at lower IFT. However, the authors did not discuss the observations, nor did they reveal the mechanisms involved. Only a few studies investigated the patterns of two-phase displacement at ultralow IFT on the level of individual pores (Pei et al. 2011; Dong et al. 2012; Gong et al. 2016). Although the ultralow IFT displacement has been observed to manifest as drainage in some of these studies, no reasonable explanation has been given. The novelty of this study is to reveal the effects of dynamic contact angle on ultralow IFT surfactant flooding by visualizing the fluid-fluid displacement in microfluidic chips.

A microemulsion is a thermodynamically stable mixture of water and oil stabilized by amphiphiles (Reed and Healy 1977). Because the free energy of microemulsion is lower than that of the separated phases, the microemulsion will form spontaneously once the surfactant solution and oil come into contact with one another (McClements 2012). Hence, the residual oil can be solubilized by micellar and flow with injected fluid, which is considered to be an important mechanism for enhancing oil recovery (Reed and Healy 1977; Javanbakht and Goual 2016). As a result, the third phase, microemulsion, is introduced into the displacement process, further complicating the flow dynamics in porous media. Pore scale studies by coinjecting surfactant solution and oil into micromodels indicate that the microemulsion is produced at the oil/water interface and then flows along with the other two phases (Unsal et al. 2016; Tagavifar et al. 2017). Xu et al. (2017a) demonstrated that the microemulsion is formed from the residual oil during surfactant flooding, which means that the microemulsion does not keep up with the same pace of the displacement front. The details of how the microemulsion affects the displacement process and phase distribution in porous media is still unclear. Typically, in water-wet reservoirs it is considered that the excess brine is the wetting phase compared to microemulsion, and the microemulsion is the wetting phase compared to oil (Hirasaki et al. 1983). By applying the wetting preference of each phase, the phase distribution in porous media can be obtained. However, as mentioned previously, the viscous forces dominate capillary forces at ultralow IFT, so the phase distribution and displacement pattern can be strongly affected by the viscous forces and are more complex than expected.

In this study, the ultralow IFT displacement is investigated at pore scale by using a 2.5D glass micromodel. The fabrication method of the 2.5D micromodel is proposed by Xu et al. (2017a). The pore throats are etched shallower than the pore bodies, so that both the grains and pore bodies are connected. Therefore, this 2.5D pore configuration is a better analog of subsurface porous media, thus allowing displacement dynamics and phase distribution to be studied in a more realistic context (Du et al. 2020). The pore-scale displacement event, capillary snap-off, is important for the flow and trapping of nonwetting phases and can be observed in 2.5D micromodels, which is difficult to achieve in 2D micromodels. The micromodels were initially filled with hexadecane colored by an oil red dye, and then a surfactant solution was injected from one end to study the displacement process. A microscope was used to observe the flow dynamics in pore scale, and then the pore-scale events during displacement process were revealed.

## Materials and Methods

**Materials.** Hexadecane (purity = 99.0%) was purchased commercially and used as oil in this experiment. A surfactant system was developed to achieve an ultralow IFT between surfactant solution and hexadecane and consisted of anionic surfactant, cosolvent, and salt. Our anionic surfactant was monoalkyl  $C_{14}$ - $C_{15}$  branched propoxy sulfate; our cosolvent was isopropyl alcohol (IPA, purity  $\geq 99.7\%$ ); and sodium chloride (NaCl; purity  $\geq 99.0\%$ ) was used as a dye.

**Phase Behavior Experiment.** Phase behavior tests are conducted to identify the optimum salinity to obtain the lowest IFT. By gradually increasing the salinity, the phase behavior transitions from Type I to Type III to Type II, and the Type III microemulsion indicates the lowest IFT (Healy et al. 1976; Levitt et al. 2009). The surfactant solution consists of 6.0-wt% anionic surfactant monoalkyl  $C_{14}$ - $C_{15}$  branched propoxy sulfate, 5.0-wt% IPA, and NaCl with varied concentration. A 5.0-cm<sup>3</sup> surfactant solution and 5.0-cm<sup>3</sup> hexadecane were added to a graduated test tube, and then the sample was well mixed. The samples were then placed at room temperature (21°C) to observe the phase behavior, and the solubilization ratios of oil  $\sigma_O$  and water  $\sigma_W$  were calculated. For the ultralow IFT determination, the theoretical relationship developed by Huh (1979) was used to estimate the IFT, and the Chun-Huh equation is as follows:

$$\gamma = \frac{C}{\sigma^2}, \dots \dots \dots (1)$$

where  $C$  is a constant and approximately equals 0.3 mN/m.

**Viscosity Measurement.** The viscosity ratio of the invading fluid and defending fluid ( $M = \mu_I/\mu_D$ ) is usually used to characterize the favorability of two-phase displacement (Lenormand et al. 1988). Therefore, the viscosities of hexadecane, 2.0-wt% surfactant solution, 6.0-wt% surfactant solution, and the Type III microemulsion were measured by a commercial rheometer with double-gap Couette geometry. The rotational measurement was conducted to determine the viscosities, and the viscosities were plotted against shear rate. The shear rates for all measurements were gradually increased from 1 to 1000 s<sup>-1</sup>, and the measurements were conducted at the temperature of 21°C.

**Fluid-Fluid Displacement in 2.5D Micromodels.** In-house fabricated homogenous 2.5D micromodels (Fig. 1) are provided by the University of Texas at Austin and used to investigate the multiphase displacement, and the properties of the 2.5D micromodel are shown in Table 1. The pore network was etched by hydrofluoric acid on a glass chip and then fused with another glass chip. The micromodel is initially strongly water-wet without wettability modification by chemical treatment; meanwhile, the surfactant and oil used in this experiment cannot alter the micromodel from water-wet to oil-wet. The micromodel was first fully saturated with hexadecane to make sure there is no air trapped. After the saturation of oil was completed, the surfactant solution was injected by a syringe pump at the flow rate of 0.1 μL/min. A microscope with camera was used to observe the pore-scale displacement in the micromodel. The entire displacement process was monitored, and images important for illustrating displacement patterns and dynamics were taken. A digital camera with macrolens was used to capture the whole picture of displacements in the micromodels. The direction of flow in all figures is from the left to the right. After each experiment, the micromodel was cleaned by injecting petroleum ether, reagent alcohol, and deionized water in a sequence to remove any remains. Then the micromodel was dried on a hot plate at the temperature of 110°C.

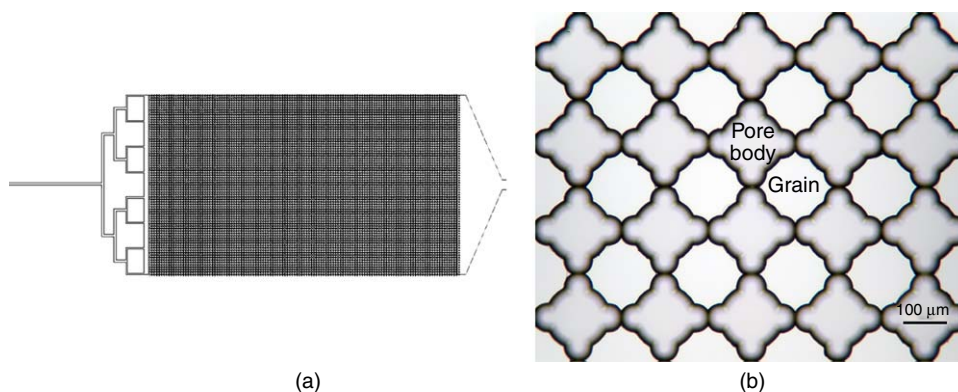


Fig. 1—(a) Schematic of the 2.5D micromodel; and (b) microscopic image of the 2.5D micromodel.

Micromodel length	2.5 cm
Micromodel width	1.5 cm
Pore body width	200 μm
Pore body depth	≈ 21 μm
Pore throat width	30 μm
Pore throat depth	≈ 5 μm
Porosity	56%

Table 1—Properties of the 2.5D micromodel.

## Results and Discussion

**Microemulsion Phase Behavior.** Because the lowest oil/water IFT can be obtained in the Type III microemulsion region, a salinity scan was conducted to determine the salinity required for the Type III microemulsion. The surfactant concentrations were 6.0 and 2.0 wt%, and the IPA concentration was at 5.0 wt%. The NaCl concentration was increased with the increment of 0.1 wt%. Fig. 2 shows the change of solubilization ratios of oil and water by varying NaCl concentration. It can be seen that the optimum salinity of 6.0-wt% surfactant is approximately 5.9 wt%, and the optimum salinity of 2.0-wt% surfactant is approximately 6.1 wt%, so 6.0- and 2.0-wt% surfactant solutions were prepared with 5.9- and 6.1-wt% NaCl for the following experiments. By using the Chun-Huh equation, the IFTs of microemulsion/oil and microemulsion/water were calculated to be approximately  $3.0 \times 10^{-3}$  and  $2.3 \times 10^{-3}$  mN/m at surfactant concentrations of 6.0- and 2.0-wt%, respectively, which are in the ultralow regime. Based on thermodynamics, the oil/water IFT should be less than the sum of the oil/microemulsion IFT and water/microemulsion IFT (Smith and Covatch 1990). Therefore, the oil/water IFT is estimated to be on the order of  $10^{-3}$  mN/m.

The formation of the microemulsion during oil/water two-phase displacement in porous media is expected to affect the displacement process because it changes the two-phase displacement to a three-phase displacement, and the ratio of microemulsion volume to total volume of oil and water ( $\beta = V_{ME}/V_T$ ) is an important factor. Typically, static tests are used to characterize the microemulsion phase behavior under equilibrium conditions (Lu et al. 2014b). However, the formation of microemulsion in porous media under a dynamic condition could be significantly different from that under a static condition. For example, the microemulsion could be under a nonequilibrium condition, and the volume of microemulsion under a dynamic condition could be less than that of the static condition (Tagavifar et al. 2017). To investigate the difference of microemulsion formation under static and dynamic conditions and the effects of microemulsion formation on the displacement patterns, solutions with surfactant concentrations of 2.0 and 6.0 wt% were used in the experiments. Based on the experimental results, the  $\beta$  of static phase behavior were calculated to be 58.5 and 23.0% for 6.0- and 2.0-wt% surfactant, respectively.

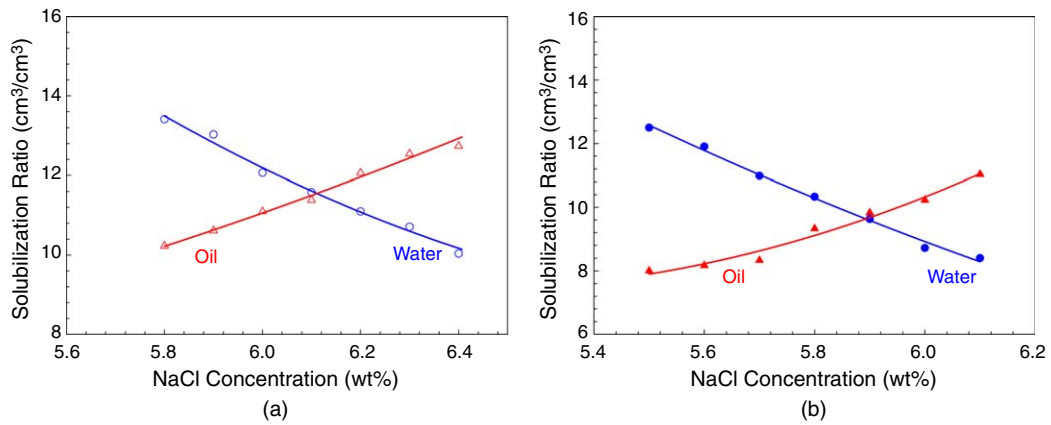


Fig. 2—Microemulsion phase behaviors of (a) 2.0-wt% surfactant and (b) 6.0-wt% surfactant.

**Dynamic Contact Angle during Displacement at Ultralow IFT.** Surfactant solution was injected into the micromodel with a flow rate of 0.1  $\mu\text{L}/\text{min}$  (interstitial velocity of 2.679 ft/D) to displace oil. Fig. 3 shows the displacement front in the conduit before entering the porous medium. As previously mentioned, the micromodel is strongly water-wet initially, and the shape of the meniscus (Fig. 3a) is concave when oil is displaced by water at high IFT. However, as shown in Figs. 3b and 3c, the menisci are convex, which seems to indicate the micromodel is strongly oil-wet rather than water-wet. Typically, the contact angle is measured under a static condition and is a balance of solid/oil, solid/water, and oil/water IFTs, which is given by Young's equation (Young 1805):

$$\cos\theta_s = \frac{\gamma_{so} - \gamma_{sw}}{\gamma_{wo}}, \dots\dots\dots (2)$$

where  $\theta_s$  is the static contact angle, and  $\gamma_{so}$ ,  $\gamma_{sw}$ , and  $\gamma_{wo}$  are solid/oil, solid/water, and oil/water IFTs, respectively.

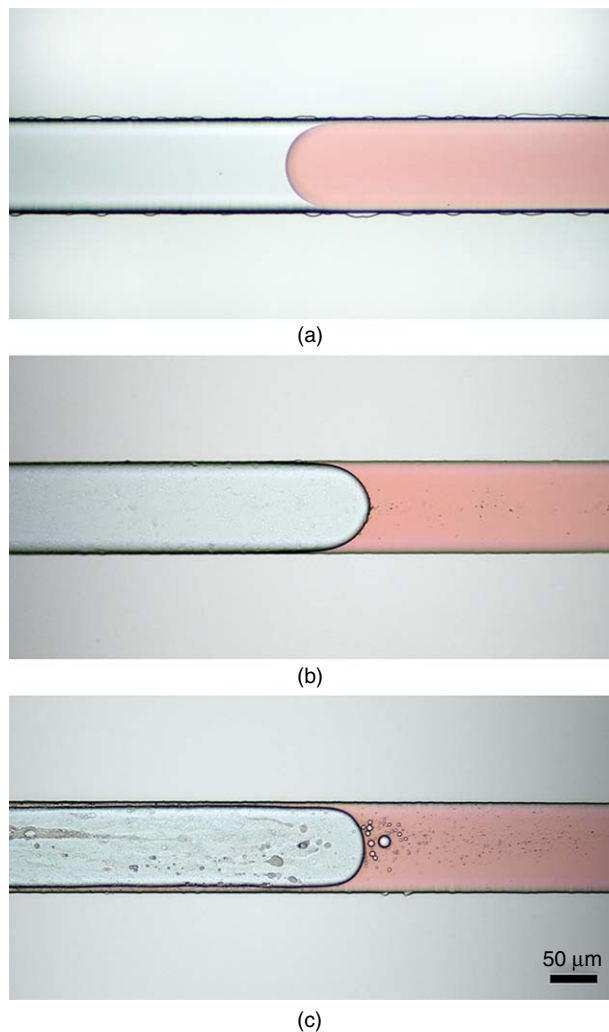


Fig. 3—Advancing of oil/water/surfactant solution interface in the conduit: (a) water, (b) 2% surfactant, and (c) 6% surfactant. The clear invading phase is the water/surfactant solution, and the red defending phase is oil. The flow direction is from left to right.

However, the contact angle under dynamic conditions can deviate significantly from that under a static condition. The shape of the oil/water meniscus is determined by the balance between Laplace pressure and normal stress difference across the meniscus (Hansen and Toong 1971; Levaché and Bartolo 2014). The governing equation of the meniscus shape can be expressed as

$$\gamma k(s) = \Delta\tau, \dots\dots\dots (3)$$

where  $\gamma$  is the IFT,  $k(s)$  is the local interface curvature,  $s$  is the curvilinear coordinate, and  $\Delta\tau$  is the normal stress difference. Eq. 3 was coupled with the Stokes equation to solve for meniscus shape, and Huh-Scriven velocity fields of wedge flow was applied (Huh and Scriven 1971). Then the following differential equation governing the meniscus shape can be derived (Chan et al. 2013; Levaché and Bartolo 2014):

$$\frac{d^2\theta}{ds^2} = \frac{3Ca}{h(h + 3\lambda_s)} f(\theta, M), \dots\dots\dots (4)$$

where

$$f(\theta, M) \equiv \frac{2\sin^3\theta[f_1(\theta)/M^2 + 2f_3(\theta)/M + f_1(\pi - \theta)]}{3[f_1(\theta)f_2(\pi - \theta)/M - f_1(\pi - \theta)f_2(\theta)]},$$

$$f_1(\theta) = \theta^2 - \sin^2\theta,$$

$$f_2(\theta) = \theta - \sin\theta\cos\theta,$$

$$f_3(\theta) = [(\theta(\pi - \theta) + \sin^2\theta)], \dots\dots\dots (5)$$

where  $\theta$  is the local interface angle;  $h$  is the distance between meniscus and conduit wall; and  $\lambda_s \ll H$  is the slip length at the wall, which is used to regularize the stress singularity at the wall. Because the solutions are not sensitive to the slip length  $\lambda_s$ , here we set  $\lambda_s = 1.0 \times 10^{-5}$ . The boundary conditions are given as follows:

$$h(s = 0) = 0, \quad h(s = 1) = 0.5, \quad \theta(s = 0) = \theta_s, \quad \theta(s = 1) = \frac{\pi}{2}. \dots\dots\dots (6)$$

The preceding equation can be solved to obtain the shape of oil/water meniscus. The dynamic contact angle increases with  $Ca$ , and it can reach  $180^\circ$  when  $Ca$  is above a critical value. The evolution of the dynamic contact angle with the capillary number has been proven by several experimental studies, and the variation of  $Ca$  was often achieved by changing the viscosity of invading phase and flow rate (Hoffman 1975; Fermigier and Jenffer 1991). In our study, the increase of  $Ca$  was obtained by reducing the IFT, and the similar change of dynamic contact angle was observed. Once the  $Ca$  is above the critical value, the velocity of three-phase contact line is lower than that of the meniscus leading to the contact line instability (Marchand et al. 2012). As a consequence, the displacement is incomplete, and the defending phase remains on the tube wall in the form of macroscopic film.

It can be seen from Fig. 3 that both menisci are convex for surfactant concentrations of 2.0 and 6.0 wt%. The contact line was still stable for the advancement of 2.0-wt% surfactant solution, whereas the contact line was unstable for the advancement of 6.0-wt% surfactant solution, which leads to the entrainment of the oil film. Fig. 4 shows the viscosities of 2.0- and 6.0-wt% surfactant solutions. The 6.0-wt% surfactant solution has much higher viscosity than that of 2.0-wt% surfactant solution at low shear rates. The surfactant solutions showed a non-Newtonian rheological behavior, and the viscosities reduced with the increase of shear rate, especially for the 6.0-wt% surfactant solution. The high viscosity and non-Newtonian behavior of the 6.0-wt% surfactant solution could be attributed to the formation of wormlike micelles. Because the surfactant concentration is high, the presence of short chain alcohols and NaCl can promote the formation of wormlike micelles (Chen et al. 2019). It can also be noticed that the microemulsion exhibited a desired Newtonian behavior over a wide range of shear rates, and this is because of the presence of short-chain alcohols. The short-chain alcohols can reduce the viscosity of microemulsion and promote the Newtonian behavior (Tagavifar et al. 2018). Because the  $Ca$  increases with the increase of viscosity of invading phase, the  $Ca$  of invading of 6.0-wt% surfactant solution can be one or two magnitudes higher than that of the invading 2.0-wt% surfactant solution. To estimate the capillary number during displacement process, the viscosities of 2.0- and 6.0-wt% surfactant solutions during displacement need to be obtained. Because the viscosities are shear-rate dependent, the shear rate  $\dot{\gamma}$  in the conduit is used to get the corresponding viscosity. The shear rate at the inner walls of a power-law fluid flowing within the conduit is (Giles et al. 2004):

$$\dot{\gamma} = \frac{\left(\frac{2}{n} + 4\right)Q}{wh^2}, \dots\dots\dots (7)$$

where  $n$  is the flow behavior index of power-law fluid,  $Q$  is the flow rate, and  $w$  and  $h$  are the width and height of the conduit, respectively. The flow behavior index  $n$  of 2.0- and 6.0-wt% surfactant solutions are determined to be 0.935 and 0.473, respectively. Then  $\dot{\gamma}$  are calculated to be 29.00 and 38.87  $s^{-1}$  for 2.0- and 6.0-wt% surfactant solutions at the flow rate of 0.1  $\mu\text{L}/\text{min}$ . Therefore, the viscosities of 2.0- and 6.0-wt% surfactant solutions during displacement are 4.1 and 35.0 mPa·s, respectively. Finally, if we assume the IFT between oil and surfactant solution is  $3.0 \times 10^{-3}$  mN/m, then the capillary numbers can be approximately calculated to be  $1.3 \times 10^{-2}$  and  $1.1 \times 10^{-1}$  for invading of 2.0- and 6.0-wt% surfactant solutions, respectively.

The evolution of the meniscus shape with the increase of  $Ca$  is obtained by numerically solving Eq. 4 using the MATLAB® (The MathWorks, Inc., Natick, Massachusetts, USA) BVP4C method. Here we show the meniscus profile of 6.0-wt% surfactant solution/oil in Fig. 5. The static contact angle is assumed to be  $0^\circ$  because the micromodel is strongly water-wet, and  $M$  is calculated to be 10.3. The meniscus changes from concave to convex with the increase of capillary number. When the capillary number is small, the apparent contact angle increases slightly with increasing the capillary number and is still close to  $0^\circ$ . A rapid increase of apparent contact angle can be observed when the capillary number is higher, and the meniscus changes from concave to convex. No stationary solution can be found when the  $Ca$  is higher than  $9.0 \times 10^{-2}$ , which means that the wetting transition occurs. This is in a good agreement with experimental results, where the oil entrainment has already happened when the  $Ca$  is  $1.1 \times 10^{-1}$ . Dong et al. (2012) and Pei et al. (2011) observed that the alkaline solution penetrated into the oil phase during alkaline flooding in a water-wet micromodel. But they attributed this phenomenon to the low oil/water IFT rather than the contact line instability.

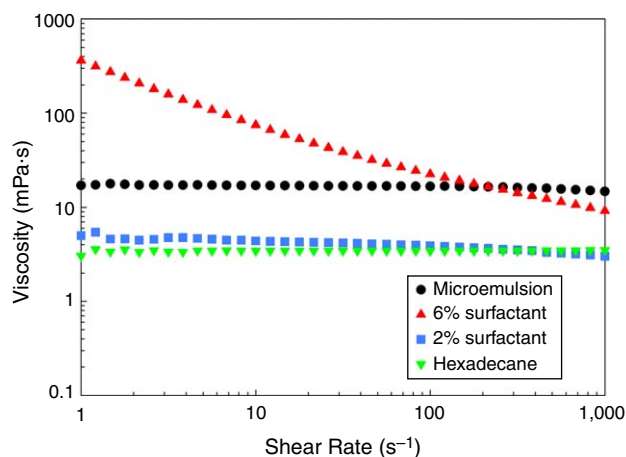


Fig. 4—Viscosities of microemulsion (prepared with 6.0-wt% surfactant), 6.0-wt% surfactant solution, 2.0-wt% surfactant solution, and hexadecane. The salinities of surfactant solutions are at optimum.

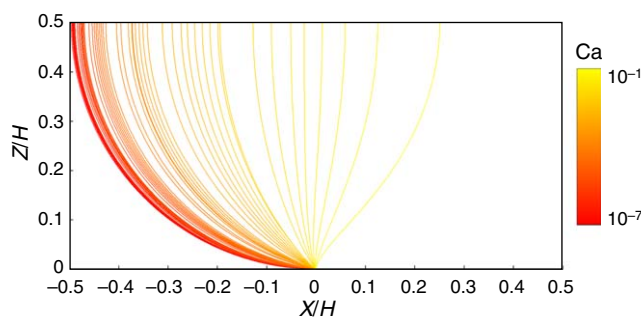


Fig. 5—Evolution of the shape of the oil/water meniscus with the increase of capillary number ( $M = 10.3$ ).

Fig. 6 shows the initial stage of oil displaced by surfactant solutions in the micromodel. The surfactant solution/oil menisci are all convex in the displacement process, which is the same as the observation in the conduit. Similar phenomena were also found in the study by Liang et al. (2020). After the meniscus passed a pore, a part of oil was left on the pore surface, and the pattern of advancement of meniscus and distribution of residual oil is similar to the oil/water displacement in an oil-wet micromodel (Du et al. 2020). The displacement patterns in both the conduit and porous medium show that the displacement process is dominated by the dynamic contact angle rather than the static contact angle at high capillary number achieved by reducing IFT to an ultralow level, regardless of whether the micromodel is water-wet or oil-wet. The displacement of surfactant solution by oil was also conducted and is shown in Fig. 7. Because the viscosity of oil is lower than the viscosities of 2.0- and 6.0-wt% surfactant solutions, viscous fingering occurred during displacements, especially when oil displaced the 6.0-wt% surfactant solution. The displacement patterns were similar to those when oil was displaced by surfactant solutions. The shape of the oil/water meniscus was convex, and a large part of surfactant solution was bypassed by the oil. To better assess the overall displacement pattern, images of the entire micromodel during surfactant flooding are shown in Fig. 8. It can be observed that the displacement is more stable at the surfactant concentration of 6.0 wt% because the viscosity of 6.0-wt% surfactant solution is much higher than the viscosity of 2.0-wt% surfactant solution. As a result, less oil was left when the 6.0-wt% surfactant solution reached the outlet of the micromodel. Moreover, owing to the contact line instability, part of the oil was left behind by the displacement front and then flowed with the injected surfactant solution. By comparing Figs. 8a, 8c, and 8e with Figs. 8b, 8d, and 8f, we can see that there is more residual phase behind the displacement front at the surfactant concentration of 6.0 wt%. This is due to the lower pore-scale displacement efficiency at a surfactant concentration of 6.0 wt% than at a surfactant concentration of 2.0 wt%, as well as the emulsification of the residual oil to form a microemulsion, which further increases the volume of the residual phase. After all the continuous oil is recovered, there is still a significant amount of residual oil and microemulsion left in the model. Hence, the pore-scale displacement is not particularly efficient at the ultralow IFT because of the contact line instability. The flow of residual oil and microemulsion is driven by pressure and shear forces exerted by the injected surfactant solution, so the continuous injection of surfactant solution is required to recover all residual oil and microemulsion. Therefore, it is possible to improve the efficiency of surfactant flooding by controlling the capillary number below the critical value.

It is a common practice to use surfactant to improve oil recovery by reducing IFT to ultralow, and the wettability alteration is also considered to be an important mechanism of enhanced oil recovery (Gupta and Mohanty 2008; Babu et al. 2015; Kumar and Mandal 2016). The displacement pattern observed in this study could question the idea of wettability alteration during ultralow IFT flooding because the displacement process is governed by the dynamic contact angle, which could be greater than  $90^\circ$  at the typical displacement velocity. For example, if a dilute surfactant solution that produces ultralow IFT with oil is injected continuously into water-wet reservoir, the dynamic contact angle could be greater than  $90^\circ$ , which makes the displacement appear to be drainage. The contact line instability could occur in the near-wellbore region because of the higher velocity. In this case, wettability alteration does not have a significant effect on the displacement, at least at the displacement front, unless the flow rate is slow enough, which would offset the effect of IFT reduction.

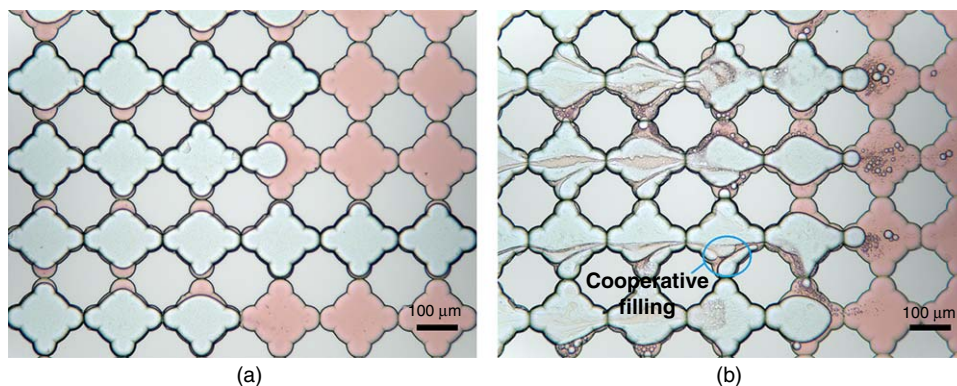


Fig. 6—Initial stage of oil displaced by surfactant solution: (a) 2.0-wt% surfactant and (b) 6.0-wt% surfactant.

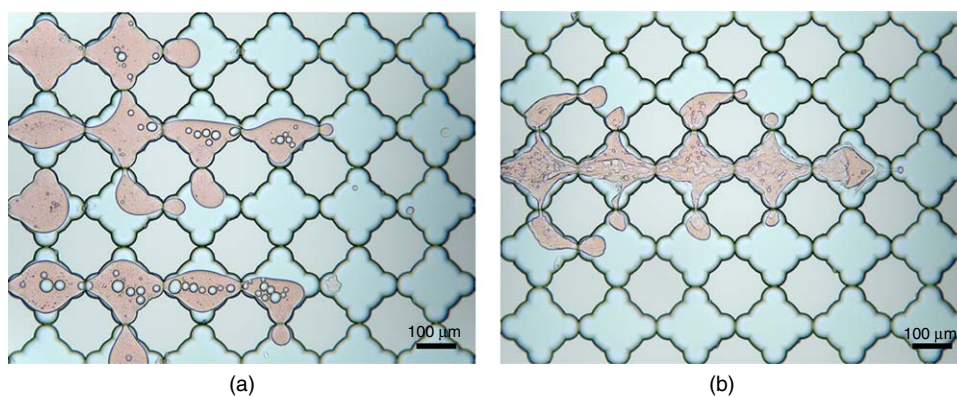


Fig. 7—Initial stage of surfactant solution displaced by oil: (a) 2.0-wt% surfactant and (b) 6.0-wt% surfactant.

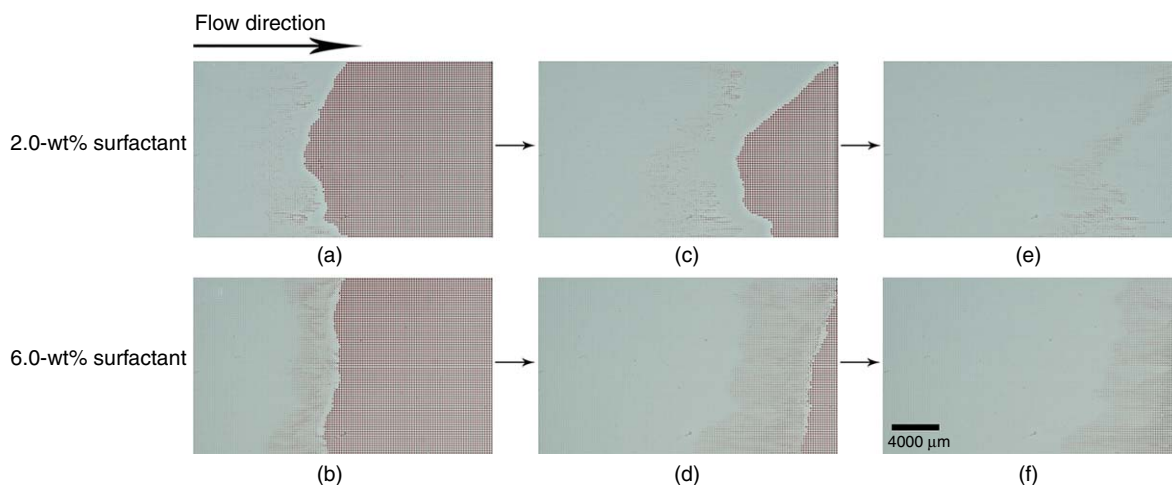
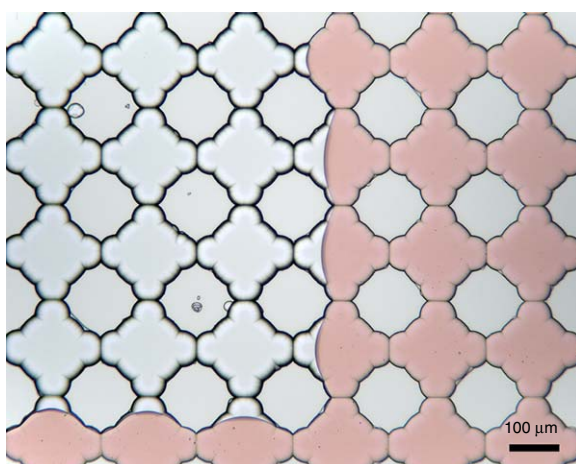


Fig. 8—Images of the entire micromodel during surfactant flooding: (a) and (b) the displacement front reached the middle of the micromodel; (c) and (d) the displacement front reached the outlet of the micromodel; (e) and (f) all the continuous oil was recovered. The grayish red phases shown in (e) and (f) are the residual oil and the microemulsion formed from residual oil, respectively.

In field applications, the surfactant solution is injected into the reservoir as a slug. Because the shape of the meniscus is determined by the capillary number, the meniscus shape will change if the surfactant is consumed during displacement. The capillary number is low after the surfactant in solution is exhausted; therefore, the viscous forces are not large enough to significantly distort the shape of the oil/water interface. We injected a slug of 2.0-wt% surfactant solution into the micromodel, and the menisci after the surfactant slug traveled a certain distance in the micromodel are shown in Fig. 9. Comparison of Figs. 6 and 9 shows that the displacement processes are quite different for high and low capillary numbers. Because the salinity in the surfactant solution is at optimum, the surfactant in water phase has a high tendency to diffuse into the oil phase to form the Type III microemulsion. It is generally accepted that the Type III microemulsion coexists with almost pure brine and pure oil under equilibrium conditions (Andelman et al. 1987). The slug of surfactant solution was surrounded by oil, and then the surfactant concentration was reduced due to diffusion into the oil phase during flow.

Finally, the surfactant in solution was exhausted, which led to the significant increase of the oil/water IFT. As shown in Fig. 9, the shape of oil/water meniscus is concave as a result of the high IFT that the displacement process is dominated by the capillary forces rather than the viscous forces. The capillary number was reduced by approximately five orders of magnitude after the surfactant was exhausted, so the dynamic contact angle is close to the static contact angle.



**Fig. 9**—Oil/water menisci changed from convex to concave after the surfactant in water phase was exhausted.

**Formation of Microemulsion in Micromodel.** As shown in Fig. 6b, the Type III microemulsion started to form once the 6.0-wt% surfactant solution invaded into the micromodel. The light orange color microemulsion was formed from the residual oil, and no visible microemulsion was formed at the front interfaces, which is also consistent with that observed by Liang et al. (2020). The cooperative filling indicates the overlap of menisci in multiple pores, which reduces the number of menisci and smooths the fluid/fluid interface. The cooperative pore filling between two adjacent pores makes the residual oil form an oil film. Owing to the ultralow IFT, the oil film can be elongated and become thinner. During this process, the oil film spontaneously emulsified and gradually changed into a microemulsion. In comparison, less microemulsion was formed from the bypassed residual oil that resided in the pore throat. The spontaneous emulsification is a process of diffusion and nucleation driven by the chemical gradient between oil and water phases (Miller 1988; Nishimi and Miller 2000). Surfactants, alcohols, and water diffuse into the oil phase to form the microemulsion phase. The rate of the emulsification process is limited by chemical gradient of surfactants and the specific area of oil. The large specific surface ratio of the oil film promotes the diffusion and emulsification, whereas the low specific surface ratio of the residual oil in the pore throat limits the emulsification process. This could explain why the microemulsion was mainly formed from the oil film, and the cooperative pore filling event is important for the microemulsion formation.

**Fig. 10** shows the microemulsion in the micromodel after 0.5 pore volumes of surfactant solution was injected. The volume of microemulsion formed during displacement process of 2.0-wt% surfactant solution was much less than that of 6.0-wt% surfactant solution. Only a few upstream pores were partially occupied by microemulsion as shown in Fig. 10a, and the microemulsion formed during dynamic displacement is less than that formed during the static phase behavior experiment. In the static phase behavior experiments, the oil and surfactant solution are fully mixed and have enough time to form microemulsion. However, convection and diffusion play important roles in emulsification in the displacement process. As mentioned previously, the emulsification is limited by diffusion, which can be described by Fick's law. The convection provides high concentration gradients near the interfaces, promoting the diffusion. The higher surfactant concentration in the water phase leads to a faster diffusion (Nishimi and Miller 2000). It will take longer time for the surfactant concentration in the oil to reach the concentration required for emulsification if the surfactant concentration in the water phase is lower. Because the residence time of the two displacements is the same, more microemulsion was produced when the oil was displaced by a 6.0-wt% surfactant solution.

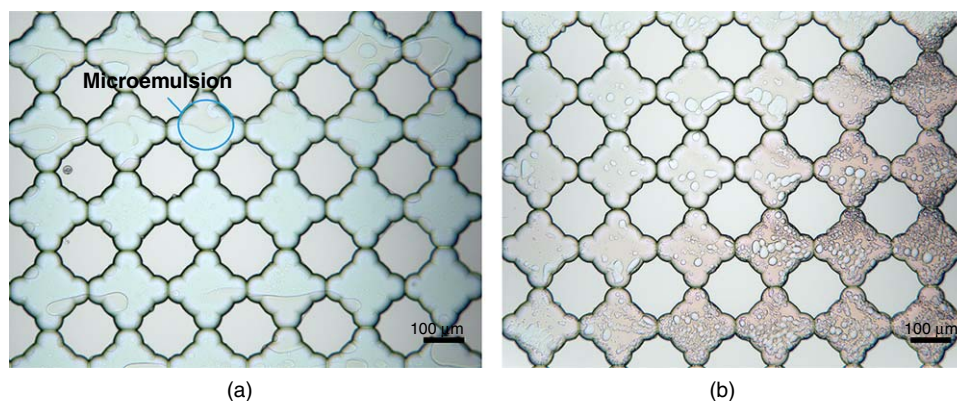


**Fig. 10**—Microemulsion formed in micromodel during displacements at surfactant concentrations of (a) 2.0 wt% and (b) 6.0 wt%. Discontinuous microemulsion existed in some of the pores at the surfactant concentration of 2.0 wt%. The microemulsion occupied entire pores at the surfactant concentration of 6.0 wt%, making the injected surfactant solution discontinuous.

The oil/water ratio of microemulsion obtained in the static phase behavior experiment is fixed at a certain salinity and certain alcohol concentration. However, the microemulsion formed in the micromodel has different colors, as shown in Fig. 9b, meaning the in-situ oil/water ratio of the microemulsion varies at different locations. The dark color microemulsion is rich in oil, and the light color microemulsion is rich in water. The microemulsion formed under dynamic conditions is not at equilibrium because it is continuously in contact with the fresh surfactant solution. The oil content in the microemulsion increases as it gets closer to the displacement front, and this attributes to the variation of the surfactant to alcohol ratio (Tagavifar et al. 2017). IPA is a hydrophilic, short-chain alcohol, and it is also soluble in oil. Due to the diffusion of IPA into the oil during the displacement, the concentration of IPA in the solution near the front edge is relatively low, making the surfactant more lipophilic. As a result, the microemulsion in the front has a higher oil content and a darker color. It is noteworthy that although the oil content in microemulsion increased from left to right as shown in Fig. 10b, the microemulsion still existed as a single phase.

Although the ultralow IFT displacement is dominated by viscous forces, the dynamic contact angle is significantly larger than the static contact angle at the displacement front. The static contact angle still plays a role in upstream phase distribution (Broens and Unsal 2018). As shown in Fig. 10a, some fine microemulsion droplets adhered to the grain surface with a regular shape. In the scenario, the wettability of grains rather than viscous forces determines the three-phase contact angle.

**Displacement Behavior in the Presence of Microemulsion.** The formation of a microemulsion during the process of oil displaced by 6.0-wt% surfactant solution at flow rate of 0.1  $\mu\text{L}/\text{min}$  can significantly affect the flow dynamics. At the early stage of displacement (Fig. 6b), only a small amount of microemulsion was formed, and then the microemulsion flowed together with the surfactant solution. The microemulsion did not significantly affect the displacement process at this moment, and the surfactant solution was still continuous. More microemulsion was formed as the displacement continued, then a microemulsion bank formed behind the displacement front. From there on, the surfactant solution flowed through the microemulsion as a discontinuous phase that was similar to the bubble flow in traditional two-phase flow theory (Fig. 10b). The main reason for this phenomenon is the extremely low IFT between surfactant solution and microemulsion. The Type III microemulsion is in equilibrium with excess oil and brine with almost no surfactant. The equilibrium is broken if the microemulsion is in contact with the fresh surfactant solution, and it approaches a new equilibrium. The IFT between microemulsion and surfactant solution could be very low because the composition of each phase is approaching one another (Hirasaki et al. 1983). This makes the contact line unstable and the two-phase displacement similar to a miscible displacement. The interface of microemulsion/surfactant solution was very flexible because of the extremely low IFT, and the surfactant solution was easy to form droplets by shear stress and became discontinuous during the displacement (Walstra 1993). The droplets of surfactant solution flowed with a higher velocity than that of microemulsion, which is known as slip between two phases. The surfactant solution entered the oil phase still in the form of droplets as shown in Fig. 10. The formation of the water-in-oil macroemulsion is expected to effectively control the displacement profile and increase the sweep efficiency if the displacement is performed with an unfavorable viscosity ratio (Pei et al. 2014; Xu et al. 2017b). The water-in-oil macroemulsion had a lower oil ratio on the microemulsion side and had a higher oil ratio at the displacement front.

Because the surfactant solution was not at equilibrium with the microemulsion, the surfactant and alcohol in solution continuously diffused into the microemulsion. The surfactant and alcohol concentrations in solution were reduced after passing through the microemulsion. Then the microemulsion was difficult to form between oil and the solution with low surfactant concentration within a relatively short period of time, which was similar to the case of 2.0-wt% surfactant solution. No visible microemulsion was formed between the droplets of surfactant solution and the oil as shown in Fig. 11. In this scenario, the further formation of microemulsion is due to the solubilization of oil by the existing microemulsion. This indicates that the interaction between oil and microemulsion plays an important role for enhancing oil recovery.

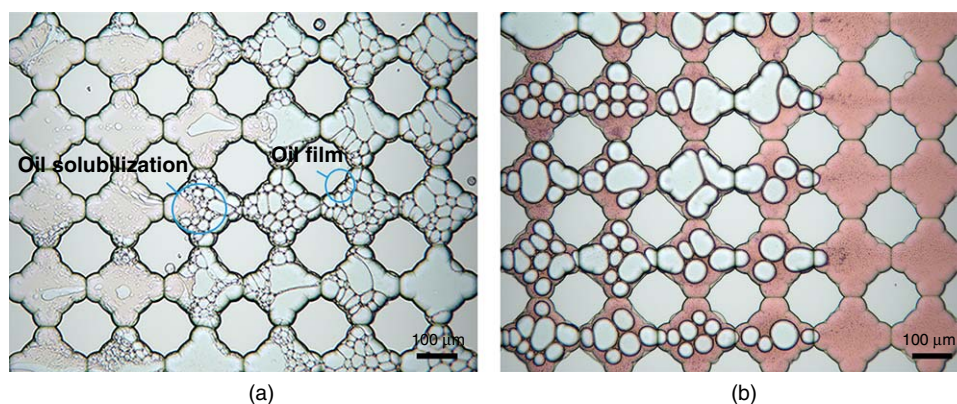


**Fig. 11—(a) Surfactant solution penetrated into the oil phase after it passed the microemulsion, and (b) the surfactant solution displaced the oil in the form of droplet. The boundary of microemulsion in the upstream (shown in Fig. 11a) is adjacent to the displacement front in the downstream (shown in Fig. 11b). The surfactant concentration in solution is 6.0 wt%.**

**Limitations and Field-Scale Implications.** The pore-scale ultralow IFT displacement pattern and its governing mechanisms are important for understanding oil and nonaqueous phase liquid recovery at large-scale and optimizing recovery strategies. Although wettability alteration has been proven to be an important mechanism for improving sweep efficiency at high IFT, the finding in our pore-scale study indicates that the ultralow IFT displacement in the reservoir appears as drainage regardless of the wettability of the reservoir. In this study, the displacements were conducted under a favorable viscosity ratio so that the fingering did not occur. However, the unfavorable viscosity ratio is often encountered in oil recovery in the field (Bryan and Kantzas 2007). The oil-wet behavior of the reservoir under ultralow IFT displacement together with the unfavorable viscosity ratio promotes viscous fingering, resulting in low oil recovery (Zhao et al. 2016). Therefore, it is critical to provide sufficient mobility control during surfactant flooding in field applications to prevent viscous fingering.

Our study also indicates that the pore-scale displacement efficiency decreased due to the contact line instability when the capillary number exceeded a critical value. Therefore, it is possible to improve the efficiency of surfactant flooding in field applications by controlling the capillary number below the critical value. At the same time, the capillary number required to mobilize oil ganglia should also be satisfied to ensure that the trapped oil can be recovered. By satisfying both conditions, or finding a balance between them, the efficiency and economy of surfactant flooding can be improved.

The micromodel used in this study is homogeneous, so that the displacement is piston-like at the favorable viscosity ratios. As a result, there is no unswept oil behind the displacement front, which makes it impossible to study the role of static contact angle on oil recovery during the ultralow IFT displacement. Therefore, we would further study the ultralow IFT displacement in a heterogeneous micromodel under unfavorable viscosity ratio to understand the contribution of static contact angle on the recovery of unswept oil far from the displacement front.

## Conclusions

Wettability is known to be an important factor in determining the displacement characteristics and oil recovery. The displacements at ultralow IFT indicate that the dynamic contact angle is significantly larger than the static contact angle. The shape of the fluid/fluid meniscus is governed by the balance between capillary forces and viscous forces. The capillary forces become very small at ultralow IFT so that the viscous forces dominate over the capillary forces, and the meniscus is distorted from concave to convex as the dynamic contact angle increases. The dynamic contact angle reaches  $180^\circ$  when the capillary number exceeds a critical value. The significant increase of dynamic contact angle at ultralow IFT changes the fluid-fluid displacement characteristics and phase distribution. Our study shows that the ultralow IFT surfactant flooding will manifest as strong drainage even in an initial strongly water-wet porous medium. In contrast, the high IFT waterflooding will show strong imbibition in the porous medium that are initially strongly water-wet.

The microemulsion is mainly formed from the residual oil. The oil film is prone to be emulsified compared to the residual oil in the pore throat, because it has a larger contact area with surfactant solution. After the microemulsion bank is formed, the surfactant solution passes through the microemulsion bank in the form of droplets rather than as a continuous phase. The extremely low IFT between surfactant solution and microemulsion made the contact line unstable during this process. The surfactant concentration decreased after the solution passed through the microemulsion. Therefore, no visible microemulsion is formed between the surfactant solution and oil at the displacement front.

The alteration of rock wettability from oil-wet to water-wet by surfactant is believed to be an important mechanism to improve oil recovery. However, the observations in this study indicate that the invasion of surfactant solution into micromodels initially filled with oil appears as strong drainage, which means the static contact angle has little impact on the displacement at the front, where the viscous forces dominate the capillary forces. Meanwhile, the static contact angle also affects the ultralow IFT displacement where the capillary number is small, such as upstream and dead-ends. Further pore-scale studies are needed to investigate the role of wettability alteration on oil recovery during surfactant flooding.

## Nomenclature

$C$	= Huh constant, mN/m
$Ca$	= capillary number, dimensionless
$h$	= height, $\mu\text{m}$
$k$	= interface curvature, dimensionless
$M$	= viscosity ratio, dimensionless
$n$	= flow behavior index, dimensionless
$Q$	= flow rate, $\mu\text{L}/\text{min}$
$s$	= the curvilinear coordinate, dimensionless
$v$	= velocity, $\text{ft}/\text{D}$
$V$	= volume, $\text{cm}^3$
$w$	= width, $\mu\text{m}$
$\beta$	= volume ratio, dimensionless
$\gamma$	= interfacial tension, mN/m
$\dot{\gamma}$	= shear rate, $\text{s}^{-1}$
$\theta$	= angle, rad
$\lambda_s$	= slip length, dimensionless
$\mu$	= viscosity, $\text{mPa}\cdot\text{s}$
$\sigma$	= solubilization ratio, dimensionless
$\tau$	= normal stress, dimensionless

## Acknowledgments

Jun Lu, Weipeng Yang, and Chenliang Fu acknowledge the McDougall School of Petroleum Engineering at the University of Tulsa for the support of this research. Matthew T. Balhoff and Yujing Du acknowledge the Chemical EOR Industrial Affiliates Project in the Center for Subsurface Energy and the Environment at the University of Texas at Austin for the financial support of this research and thank the Hildebrand Department of Petroleum and Geosystems Engineering at the University of Texas at Austin.

## References

- Abedi, B., Castaño, E. P. M., Heidaryan, E. et al. 2020. Pore-Scale Visualization on Polymer Flooding: Application of Singular Value Decomposition-Based Image Analysis Method. *J Porous Media* **23** (6): 531–543. <https://doi.org/10.1615/JPorMedia.2020033831>.
- Andelman, D., Cates, M. E., Roux, D. et al. 1987. Structure and Phase Equilibria of Microemulsions. *J Chem Phys* **87** (12): 7229–7241. <https://doi.org/10.1063/1.453367>.
- Babu, K., Pal, N., Bera, A. et al. 2015. Studies on Interfacial Tension and Contact Angle of Synthesized Surfactant and Polymeric from Castor Oil for Enhanced Oil Recovery. *Appl Surf Sci* **353**: 1126–1136. <https://doi.org/10.1016/j.apsusc.2015.06.196>.
- Bartels, W.-B., Mahani, H., Berg, S. et al. 2017. Oil Configuration under High-Salinity and Low-Salinity Conditions at Pore Scale: A Parametric Investigation by Use of a Single-Channel Micromodel. *SPE J.* **22** (5): 1362–1373. SPE-181386-PA. <https://doi.org/10.2118/181386-PA>.

- Blake, T. D., Bracke, M., and Shikhmurzaev, Y. D. 1999. Experimental Evidence of Nonlocal Hydrodynamic Influence on the Dynamic Contact Angle. *Phys Fluids* **11** (8): 1995–2007. <https://doi.org/10.1063/1.870063>.
- Broens, M. and Unsal, E. 2018. Emulsification Kinetics during Quasi-Miscible Flow in Dead-End Pores. *Adv Water Resour* **113**: 13–22. <https://doi.org/10.1016/j.advwatres.2018.01.001>.
- Bryan, J. L. and Kantzas, A. 2007. Enhanced Heavy-Oil Recovery by Alkali-Surfactant Flooding. Paper presented at the SPE Annual Technical Conference and Exhibition, Anaheim, California, USA, 11–14 November. SPE-110738-MS. <https://doi.org/10.2118/110738-MS>.
- Chan, T. S., Srivastava, S., Marchand, A. et al. 2013. Hydrodynamics of Air Entrainment by Moving Contact Lines. *Phys Fluids* **25** (7): 074105. <https://doi.org/10.1063/1.4814466>.
- Chatzis, I. and Morrow, N. R. 1984. Correlation of Capillary Number Relationships for Sandstone. *SPE J.* **24** (5): 555–562. SPE-10114-PA. <https://doi.org/10.2118/10114-PA>.
- Chen, C., Wang, S., Grady, B. P. et al. 2019. Oil-Induced Viscoelasticity in Micellar Solutions of Alkoxy Sulfate. *Langmuir* **35** (37): 12168–12179. <https://doi.org/10.1021/acs.langmuir.9b01969>.
- Cieplak, M. and Robbins, M. O. 1988. Dynamical Transition in Quasistatic Fluid Invasion in Porous Media. *Phys Rev Lett* **60** (20): 2042–2045. <https://doi.org/10.1103/PhysRevLett.60.2042>.
- Cieplak, M. and Robbins, M. O. 1990. Influence of Contact Angle on Quasistatic Fluid Invasion of Porous Media. *Phys Rev B* **41** (16): 11508–11521. <https://doi.org/10.1103/PhysRevB.41.11508>.
- Dong, M., Liu, Q., and Li, A. 2012. Displacement Mechanisms of Enhanced Heavy Oil Recovery by Alkaline Flooding in a Micromodel. *Particuology* **10** (3): 298–305. <https://doi.org/10.1016/j.partic.2011.09.008>.
- Du, Y., Mehmani, A., Xu, K. et al. 2020. Microfluidic Diagnostics of the Impact of Local Microfracture Connectivity on Hydrocarbon Recovery following Water Injection. *Water Resour Res* **56** (7): e2019WR026944. <https://doi.org/10.1029/2019WR026944>.
- Fermigier, M. and Jenffer, P. 1991. An Experimental Investigation of the Dynamic Contact Angle in Liquid-Liquid Systems. *J Colloid Interface Sci* **146** (1): 226–241. [https://doi.org/10.1016/0021-9797\(91\)90020-9](https://doi.org/10.1016/0021-9797(91)90020-9).
- Foster, W. R. 1973. A Low-Tension Waterflooding Process. *J Pet Technol* **25** (2): 205–210. SPE-3803-PA. <https://doi.org/10.2118/3803-PA>.
- Giles, H. F. Jr., Mount, E. M. III, and Wagner, J. R. Jr. 2004. *Extrusion: The Definitive Processing Guide and Handbook*. Norwich, New York, USA: William Andrew.
- Gong, H., Li, Y., Dong, M. et al. 2016. Effect of Wettability Alteration on Enhanced Heavy Oil Recovery by Alkaline Flooding. *Colloids Surf A* **488**: 28–35. <https://doi.org/10.1016/j.colsurfa.2015.09.042>.
- Gupta, R. and Mohanty, K. K. 2008. Wettability Alteration of Fractured Carbonate Reservoirs. Paper presented at the SPE Symposium on Improved Oil Recovery, Tulsa, Oklahoma, USA, 20–23 April. SPE-113407-MS. <https://doi.org/10.2118/113407-MS>.
- Hansen, R. J. and Toong, T. Y. 1971. Dynamic Contact Angle and Its Relationship to Forces of Hydrodynamic Origin. *J Colloid Interface Sci* **37** (1): 196–207. [https://doi.org/10.1016/0021-9797\(71\)90280-3](https://doi.org/10.1016/0021-9797(71)90280-3).
- Healy, R. N., Reed, R. L., and Stenmark, D. G. 1976. Multiphase Microemulsion Systems. *SPE J.* **16** (3): 147–160. SPE-5565-PA. <https://doi.org/10.2118/5565-PA>.
- Hirasaki, G., Miller, C. A., and Puerto, M. 2011. Recent Advances in Surfactant EOR. *SPE J.* **16** (4): 889–907. SPE-115386-PA. <https://doi.org/10.2118/115386-PA>.
- Hirasaki, G. J., van Domselaar, H. R., and Nelson, R. C. 1983. Evaluation of the Salinity Gradient Concept in Surfactant Flooding. *SPE J.* **23** (3): 486–500. SPE-8825-PA. <https://doi.org/10.2118/8825-PA>.
- Hoffman, R. L. 1975. A Study of the Advancing Interface. I. Interface Shape in Liquid–Gas Systems. *J Colloid Interface Sci* **50** (2): 228–241. [https://doi.org/10.1016/0021-9797\(75\)90225-8](https://doi.org/10.1016/0021-9797(75)90225-8).
- Holtzman, R. and Segre, E. 2015. Wettability Stabilizes Fluid Invasion into Porous Media via Nonlocal, Cooperative Pore Filling. *Phys Rev Lett* **115** (16): 164501. <https://doi.org/10.1103/PhysRevLett.115.164501>.
- Howe, A. M., Clarke, A., Mitchell, J. et al. 2015. Visualising Surfactant Enhanced Oil Recovery. *Colloids Surf A* **480**: 449–461. <https://doi.org/10.1016/j.colsurfa.2014.08.032>.
- Huh, C. 1979. Interfacial Tensions and Solubilizing Ability of a Microemulsion Phase that Coexists with Oil and Brine. *J Colloid Interface Sci* **71** (2): 408–426. [https://doi.org/10.1016/0021-9797\(79\)90249-2](https://doi.org/10.1016/0021-9797(79)90249-2).
- Huh, C. and Scriven, L. E. 1971. Hydrodynamic Model of Steady Movement of a Solid/Liquid/Fluid Contact Line. *J Colloid Interface Sci* **35** (1): 85–101. [https://doi.org/10.1016/0021-9797\(71\)90188-3](https://doi.org/10.1016/0021-9797(71)90188-3).
- Javanbakht, G. and Goual, L. 2016. Mobilization and Micellar Solubilization of NAPL Contaminants in Aquifer Rocks. *J Contam Hydrol* **185–186**: 61–73. <https://doi.org/10.1016/j.jconhyd.2016.01.003>.
- Johannessen, A. M. and Spildo, K. 2013. Enhanced Oil Recovery (EOR) by Combining Surfactant with Low Salinity Injection. *Energy Fuels* **27** (10): 5738–5749. <https://doi.org/10.1021/ef400596b>.
- Jung, M., Brinkmann, M., Seemann, R. et al. 2016. Wettability Controls Slow Immiscible Displacement through Local Interfacial Instabilities. *Phys Rev Fluids* **1** (7): 074202. <https://doi.org/10.1103/PhysRevFluids.1.074202>.
- Kathel, P. and Mohanty, K. K. 2013. Wettability Alteration in a Tight Oil Reservoir. *Energy Fuels* **27** (11): 6460–6468. <https://doi.org/10.1021/ef4012752>.
- Kumar, S. and Mandal, A. 2016. Studies on Interfacial Behavior and Wettability Change Phenomena by Ionic and Nonionic Surfactants in Presence of Alkalis and Salt for Enhanced Oil Recovery. *Appl Surf Sci* **372**: 42–51. <https://doi.org/10.1016/j.apsusc.2016.03.024>.
- Lenormand, R., Touboul, E., and Zarcone, C. 1988. Numerical Models and Experiments on Immiscible Displacements in Porous Media. *J Fluid Mech* **189**: 165–187. <https://doi.org/10.1017/S0022112088000953>.
- Lenormand, R., Zarcone, C., and Sarr, A. 1983. Mechanisms of the Displacement of One Fluid by Another in a Network of Capillary Ducts. *J Fluid Mech* **135**: 337–353. <https://doi.org/10.1017/S0022112083003110>.
- Levaché, B. and Bartolo, D. 2014. Revisiting the Saffman-Taylor Experiment: Imbibition Patterns and Liquid-Entrainment Transitions. *Phys Rev Lett* **113** (4): 044501. <https://doi.org/10.1103/PhysRevLett.113.044501>.
- Levitt, D., Jackson, A., Heinson, C. et al. 2009. Identification and Evaluation of High-Performance EOR Surfactants. *SPE Res Eval & Eng* **12** (2): 243–253. SPE-100089-PA. <https://doi.org/10.2118/100089-PA>.
- Liang, T., Xu, K., Lu, J. et al. 2020. Evaluating the Performance of Surfactants in Enhancing Flowback and Permeability after Hydraulic Fracturing through a Microfluidic Model. *SPE J.* **25** (1): 268–287. SPE-199346-PA. <https://doi.org/10.2118/199346-PA>.
- Lu, J., Britton, C., Solairaj, S. et al. 2014a. Novel Large-Hydrophobe Alkoxy Carboxylate Surfactants for Enhanced Oil Recovery. *SPE J.* **19** (6): 1024–1034. SPE-154261-PA. <https://doi.org/10.2118/154261-PA>.
- Lu, J., Liyanage, P. J., Solairaj, S. et al. 2014b. New Surfactant Developments for Chemical Enhanced Oil Recovery. *J Pet Sci Eng* **120**: 94–101. <https://doi.org/10.1016/j.petrol.2014.05.021>.
- Lu, J. and Pope, G. A. 2017. Optimization of Gravity-Stable Surfactant Flooding. *SPE J.* **22** (2): 480–493. SPE-174033-PA. <https://doi.org/10.2118/174033-PA>.

- Mahani, H., Keya, A. L., Berg, S. et al. 2015. Insights into the Mechanism of Wettability Alteration by Low-Salinity Flooding (LSF) in Carbonates. *Energy Fuels* **29** (3): 1352–1367. <https://doi.org/10.1021/ef5023847>.
- Marchand, A., Chan, T. S., Snoeijer, J. H. et al. 2012. Air Entrainment by Contact Lines of a Solid Plate Plunged into a Viscous Fluid. *Phys Rev Lett* **108** (20): 204501. <https://doi.org/10.1103/PhysRevLett.108.204501>.
- McClements, D. J. 2012. Nanoemulsions versus Microemulsions: Terminology, Differences, and Similarities. *Soft Matter* **8** (6): 1719–1729. <https://doi.org/10.1039/C2SM06903B>.
- Mejia, L., Tagavifar, M., Xu, K. et al. 2019. Surfactant Flooding in Oil-Wet Micromodels with High Permeability Fractures. *Fuel* **241**: 1117–1128. <https://doi.org/10.1016/j.fuel.2018.12.076>.
- Miller, C. A. 1988. Spontaneous Emulsification Produced by Diffusion—A Review. *Colloids Surf* **29** (1): 89–102. [https://doi.org/10.1016/0166-6622\(88\)80173-2](https://doi.org/10.1016/0166-6622(88)80173-2).
- Morrow, N. R. and Mason, G. 2001. Recovery of Oil by Spontaneous Imbibition. *Curr Opin Colloid Interface Sci* **6** (4): 321–337. [https://doi.org/10.1016/S1359-0294\(01\)00100-5](https://doi.org/10.1016/S1359-0294(01)00100-5).
- Ngan, C. G. and Dussan V., E. B. 1982. On the Nature of the Dynamic Contact Angle: An Experimental Study. *J Fluid Mech* **118**: 27–40. <https://doi.org/10.1017/S0022112082000949>.
- Nishimi, T. and Miller, C. A. 2000. Spontaneous Emulsification of Oil in Aerosol-OT/Water/Hydrocarbon Systems. *Langmuir* **16** (24): 9233–9241. <https://doi.org/10.1021/la0006521>.
- Pei, H., Zhang, G., Ge, J. et al. 2011. Analysis of Microscopic Displacement Mechanisms of Alkaline Flooding for Enhanced Heavy-Oil Recovery. *Energy Fuels* **25** (10): 4423–4429. <https://doi.org/10.1021/ef200605a>.
- Pei, H., Zhang, G., Ge, J. et al. 2014. Effect of the Addition of Low Molecular Weight Alcohols on Heavy Oil Recovery during Alkaline Flooding. *Ind Eng Chem Res* **53** (4): 1301–1307. <https://doi.org/10.1021/ie4028318>.
- Reed, R. L. and Healy, R. N. 1977. Some Physicochemical Aspects of Microemulsion Flooding: A Review. In *Improved Oil Recovery by Surfactant and Polymer Flooding*, ed. D. O. Shah and R. S. Schechter, 383–437. Cambridge, Massachusetts, USA: Academic Press.
- Singh, K., Jung, M., Brinkmann, M. et al. 2019. Capillary-Dominated Fluid Displacement in Porous Media. *Annu Rev Fluid Mech* **51**: 429–449. <https://doi.org/10.1146/annurev-fluid-010518-040342>.
- Smith, D. H. and Covatch, G. L. 1990. Wetting Transition in a Three-Phase Surfactant/Oil/Water Microemulsion System. *J Chem Phys* **93** (9): 6870–6874. <https://doi.org/10.1063/1.458920>.
- Tagavifar, M., Herath, S., Weerasooriya, U. P. et al. 2018. Measurement of Microemulsion Viscosity and Its Implications for Chemical Enhanced Oil Recovery. *SPE J.* **23** (1): 66–83. SPE-179672-PA. <https://doi.org/10.2118/179672-PA>.
- Tagavifar, M., Xu, K., Jang, S. H. et al. 2017. Spontaneous and Flow-Driven Interfacial Phase Change: Dynamics of Microemulsion Formation at the Pore Scale. *Langmuir* **33** (45): 13077–13086. <https://doi.org/10.1021/acs.langmuir.7b02856>.
- Unsal, E., Broens, M., and Armstrong, R. T. 2016. Pore Scale Dynamics of Microemulsion Formation. *Langmuir* **32** (28): 7096–7108. <https://doi.org/10.1021/acs.langmuir.6b00821>.
- Walstra, P. 1993. Principles of Emulsion Formation. *Chem Eng Sci* **48** (2): 333–349. [https://doi.org/10.1016/0009-2509\(93\)80021-H](https://doi.org/10.1016/0009-2509(93)80021-H).
- Xu, K., Liang, T., Zhu, P. et al. 2017a. A 2.5-D Glass Micromodel for Investigation of Multi-Phase Flow in Porous Media. *Lab Chip* **17** (4): 640–646. <https://doi.org/10.1039/C6LC01476C>.
- Xu, K., Zhu, P., Colon, T. et al. 2017b. A Microfluidic Investigation of the Synergistic Effect of Nanoparticles and Surfactants in Macro-Emulsion-Based Enhanced Oil Recovery. *SPE J.* **22** (2): 459–469. SPE-179691-PA. <https://doi.org/10.2118/179691-PA>.
- Young, T. 1805. III. An Essay on the Cohesion of Fluids. *Philos Trans. R Soc London* **95**: 65–87. <https://doi.org/10.1098/rstl.1805.0005>.
- Zhao, B., MacMinn, C. W., and Juanes, R. 2016. Wettability Control on Multiphase Flow in Patterned Microfluidics. *PNAS* **113** (37): 10251–10256. <https://doi.org/10.1073/pnas.1603387113>.
- Zhong, L., Mayer, A. S., and Pope, G. A. 2003. The Effects of Surfactant Formulation on Nonequilibrium NAPL Solubilization. *J Contam Hydrol* **60** (1–2): 55–75. [https://doi.org/10.1016/S0169-7722\(02\)00063-3](https://doi.org/10.1016/S0169-7722(02)00063-3).